

ORIGINAL ARTICLE

Electrically controlled non-volatile switching of magnetism in multiferroic heterostructures via engineered ferroelastic domain states

Ming Liu^{1,2}, Tianxiang Nan³, Jia-Mian Hu⁴, Shi-Shun Zhao¹, Ziyao Zhou¹, Chen-Ying Wang^{2,5}, Zhuang-De Jiang^{2,5}, Wei Ren^{1,2}, Zuo-Guang Ye^{1,2,6}, Long-Qing Chen⁴ and Nian X Sun^{1,3}

In this work we addressed a key challenge in realizing multiferroics-based reconfigurable magnetic devices, which is the ability to switch between distinct collective magnetic states in a reversible and stable manner with a control voltage. Three possible non-volatile switching mechanisms have been demonstrated, arising from the nature of the domain states in perovskite PZN-PT crystal that the ferroelectric polarization reversal is partially coupled to the ferroelastic strain. Electric impulse non-volatile control of magnetic anisotropy in FeGaB/PZN-PT and domain distribution of FeGaB during the ferroelectric switching have been observed, which agrees very well with simulation results. These approaches provide a platform for realizing electric impulse non-volatile tuning of the order parameters that are coupled to the lattice strain in thin-film heterostructures, showing great potentials in achieving reconfigurable, compact, light-weight and ultra-low-power electronics.

NPG Asia Materials (2016) 8, e316; doi:10.1038/am.2016.139; published online 30 September 2016

INTRODUCTION

One of the central challenges in realizing non-volatile magnetic memory devices lies in finding an energy-efficient way to switch between distinct collective magnetic states in a reversible and stable manner with a control voltage.^{1–10} Multiferroic heterostructures, simultaneously exhibiting ferromagnetism, ferroelectricity and ferroelasticity, have attracted great interest due to the strong strain-mediated magnetoelectric (ME) coupling and shown promising applications for tunable magnetic devices.^{11–29} More interestingly, in these structures, a single control parameter of voltage is used to induce a lattice strain through the converse piezoelectric effect in the ferroelectric phase, which in turn tailors the magnetic properties in the mechanically coupled magnetic phase through the magnetoelastic effect.^{25,30–41} Thus, devices made of such heterostructures are ultra-fast, compact, quiet, energy efficient and susceptible to be integrated into electronic circuits. Early efforts of developing novel multiferroic heterostructures focused on the realization of a significant magnetic tunability via a linear piezoelectric effect, whereby the lattice strain is directly proportional to the applied voltage without ferroelastic domain switching. Upon removing the voltage, the magnetic state returns to the initial state.^{30,42–45} This has been demonstrated in many

prototype ME systems, such as $\text{Y}_3\text{Fe}_5\text{O}_{12}/\text{PMN-PT}$ [$\text{Pb}(\text{Mg}_{1/3}\text{Nb}_{2/3})\text{O}_3\text{-xPbTiO}_3$],³² Terfenol-D/PZN-PT [$\text{Pb}(\text{Zn}_{1/3}\text{Nb}_{2/3})\text{O}_3\text{-xPbTiO}_3$],⁴⁶ Ni/PMN-PT,⁴⁷ $\text{Fe}_3\text{O}_4/\text{PZN-PT}(011)$,¹⁹ $\text{La}_{0.7}\text{Sr}_{0.3}\text{CoO}_3/\text{PMN-PT}(011)$ ⁴⁸ and $\text{La}_{0.7}\text{Ca}_{0.15}\text{Mn}_{0.15}\text{O}_3/\text{PMN-PT}(001)$.⁴⁹ Although these ME devices point to a pathway for realizing the manipulation of magnetism with a control voltage, reversible and non-volatile switching between distinct magnetic states using lattice strain still remains a significant challenge. In non-volatile switching, the magnetic state is retained in a stable remnant state after the control voltage was turned off.^{18,20,50–52} Furthermore, these remnant magnetic states need to be reversible upon switching the voltage. Aiming at this goal, one may use voltage-induced ferroelastic domain switching or structural phase transitions in ferroelectrics to realize non-volatile tuning of magnetic properties in multiferroic heterostructures.

There are two essential requirements to achieve non-volatile electric switching of magnetism in multiferroic heterostructures. The first one is to selectively control the ferroelastic switching pathway so as to induce significant and homogeneous changes in the magnetic properties. Second, the switched domain or the domain state after undergoing the phase transition must be sufficiently stable. The first point arises from the intrinsic nature of the domain states in the

¹Electronic Materials Research Laboratory, Key Laboratory of the Ministry of Education & International Center for Dielectric Research, Xi'an Jiaotong University, Xi'an, Shaanxi, China; ²Collaborative Innovation Center of High-End Manufacturing Equipment, Xi'an Jiaotong University, Xi'an, Shaanxi, China; ³Department of Electrical and Computer Engineering, Northeastern University, Boston, MA, USA; ⁴Department of Materials Science and Engineering, Pennsylvania State University, University Park, PA, USA; ⁵State Key Laboratory for Manufacturing Systems Engineering, Xi'an Jiaotong University, Xi'an, Shaanxi, China and ⁶Department of Chemistry and 4D LABS, Simon Fraser University, Burnaby, British Columbia, Canada

Correspondence: Professor M Liu, Electronic Materials Research Laboratory, Key Laboratory of the Ministry of Education & International Center for Dielectric Research, Xi'an Jiaotong University, 28 W. Xianning Rd., Xi'an 710049, China.

E-mail: mingliu@xjtu.edu.cn

or Professor NX Sun, Department of Electrical and Computer Engineering, Northeastern University, 360 Huntington Ave, Boston, MA 02115, USA.

E-mail: nian@ece.neu.edu

Received 13 May 2016; revised 7 July 2016; accepted 24 July 2016

ferroic phases of perovskite structure like PZN-PT (with a centrosymmetrical cubic prototype symmetry of $Pm\bar{3}m$), which are 'fully ferroelectric/partially ferroelastic' (according to Aizu's notation⁵³). In these crystals, some of the polarization reversals are associated with ferroelastic domain switching, leading to lattice strains, whereas the others are not coupled to any lattice change at all. The second requirement is also important otherwise the strain will relax. In a rhombohedral $Pb(Zn_{1/3}Nb_{2/3})O_3-xPbTiO_3$ (PZN-PT, $x=0.07$) single crystal, there are eight possible polarization directions along the body diagonals, corresponding to the four structural (ferroelastic) domains (r1, r2, r3 and r4), as shown in the schematics in the Supplementary Figure S1 (Supplementary Information). When the polarization is switched by applying an electric field along various directions, the PZN-PT either locally preserves the ferroelastic state with its electric polarization undergoing a 180° ferroelectric switching to be antiparallel to the original one or change to a different ferroelastic state (71° or 109° ferroelastic switching) with a different strain. Such ferroelectrically coupled ferroelastic switching will result in a non-volatile tuning of magnetic properties in the mechanically coupled magnetic films deposited onto PZN-PT crystal.

In this work, three possible approaches as illustrated in Supplementary Figure S1 have been undertaken to address the critical issues in realizing non-volatile switching of the magnetism in FeGaB/PZN-PT multiferroic heterostructures by an electric control. We reveal that the electric impulse-induced ferroelectric/ferroelastic domain switching and structural phase transition allows the production of two stable and reversible lattice strain states and thereby lead to a robust tuning of the distinct magnetic states. The ferroelastic switching is found to take place in 23% of the entire poled area in FeGaB/PZN-PT (001) and in 80% in FeGaB/PZN-PT (011), pointing to a more significant and homogeneous non-volatile ME coupling in FeGaB/PZN-PT (011). In addition, a giant ME coupling across the phase transition in PZN-PT (011) is obtained and non-volatile switching of magnetism is realized in the FeGaB films. We also reveal the changes in local magnetic domain configurations beneath the changes of macroscopic magnetic states using phase-field modeling. These results provide a platform for realizing electric field impulse-controlled non-volatile tuning of the order parameters that are coupled to the lattice strain in thin-film heterostructures, showing great potentials in achieving reconfigurable, compact, light-weight and ultra-low-power electronics.

MATERIALS AND METHODS

Magnetic films with the structure of $Fe_{70}Ga_{18}B_{12}(50\text{ nm})/Ti(5\text{ nm})$ are deposited onto the single-crystal ferroelectric PZN-PT substrates using the magnetron sputtering at room temperature. Phase-field simulations are performed to obtain the equilibrium magnetic domain structures under the average lattice strains resulting from ferroelectric domain switching or phase transition. The governing kinetic equation is the classical Landau-Lifshitz-Gilbert equation. A three-dimensional model of $1\ \mu\text{m} \times 1\ \mu\text{m} \times 120\text{ nm}$ (corresponding three-dimensional discretional grids: $256\Delta x \times 256\Delta y \times 60\Delta z$) is utilized to describe the present film-on-substrate system, where the top $10\Delta z$ layer, the middle $25\Delta z$ layer and the bottom $25\Delta z$ layer in the constructed model are designated as the air, FeGaB film and the PZN-PT substrate, respectively. The cell size ($\Delta x, \Delta y, \Delta z$) = (3.91, 3.91, 2 nm) is smaller than the exchange length ($l_{ex} \approx 4.08\text{ nm}$). The exchange length is calculated as $l_{ex} = \sqrt{A/(\mu_0 M_s^2/2)}$ according the definition,⁵⁴ where A is the exchange stiffness constant, μ_0 is the vacuum permeability and M_s is the saturation magnetization. For checking the dependence of cell size on the results, the in-plane cell size ($\Delta x = \Delta y$) is varied from 3.91 to 2 nm ($\Delta z = 2\text{ nm}$ in all testing cases) while the system dimension ($1\ \mu\text{m} \times 1\ \mu\text{m} \times 120\text{ nm}$) remains unchanged, and no difference was found (see details of testing results in

Supplementary Figure S8). Periodic elastic and magnetostatic boundary conditions are implemented to describe a continuous magnetic thin film. Details of using phase-field simulations to model strain-stabilized magnetic domain structure in continuous thin films can be found in ref. 55 Here we list the necessary materials parameters for simulations as follows: Young's modulus $Y = 62.4\text{ GPa}$, Poisson's ratio $\nu = 0.44$; Saturation Magnetostriction coefficient $\lambda_s = 65\text{ p.p.m.}$;⁵⁶ Saturation Magnetization $M_s = 978\text{ e.m.u. cm}^{-3}$ experimentally measured through vibrating sample magnetometer; Exchange stiffness constant of FeGa ($A = 1 \times 10^{-11}\text{ J m}^{-1}$)⁵⁷ is utilized as an approximation. To our knowledge, the magnitude of the Gilbert damping coefficient for the present amorphous FeGaB film is unavailable in the literature, however, this kinetic coefficient should not affect the magnetic domain structure at equilibrium.

Experimental procedures

A high-resolution triple axis X-ray diffractometer was used to carry out the reciprocal space mapping (RSM) measurements under various poling conditions. The magnetic hysteresis loops were measured using a vibrating sample magnetometer. The ferromagnetic resonance (FMR) was measured using an x-band (9.3 GHz) electron paramagnetic resonance system. The sample was placed in a rectangular cavity working at TE_{102} mode. External magnetic fields were sequentially applied along the [100] and [0-11] directions of the PZN-PT substrate while an external electric field was applied along the thickness direction. The angular dependences of the FMR spectra were measured with different applied electric fields with an angle increment step of 11.25° .

RESULTS AND DISCUSSION

Magnetic films with the structure of $(Fe_{80}Ga_{20})_{88}B_{12}(50\text{ nm})/Ti(5\text{ nm})$ are deposited onto the ferroelectric PZN-PT single-crystal substrates using magnetron sputtering. The FeGaB film has a large magnetostriction constant around 65 p.p.m., which favors a strong ME coupling. Figures 1a–c show the RSM patterns in the vicinity of the (-113) reflections upon applying various electric fields along the [001] direction of PZN-PT. Analysis of the RSM patterns suggests that the PZN-PT substrate holds three domains of r1, r2 and r3, (Figure 1b) and exhibits different intensities for each domain after the sample was poled vertically by a positive (along the [001] direction) electric field of 8 kV cm^{-1} . The absence of the r3 domain structure might be attributed to a slight mis-cut of the PZN-PT substrate, which is evidenced by the spot intensity distribution in the RSM patterns, where about 50% of polarizations stays as the r1 domain. Upon poling the sample with a negative field of -8 kV cm^{-1} , the polarization flips from the upward to downward direction, exhibiting different RSM patterns as shown in Figure 1c. An additional high-intensity reflection spot appears, corresponding to the r3 domain state. This suggests two possible domain switching pathways from $r1^+$ to $r3^-$ (71° polarization reversal) and from $r2^+/r4^+$ to $r3^-$ (109° polarization reversal). The reflection spot of r1 domain with a reduced intensity indicates that 180° ferroelectric switching also takes place from $r1^+$ to $r1^-$. During the polarization reversal, only the 109° ferroelastic switching produces lattice strains in the (001) plane along the two diagonal axes and thereby contributes to a sizable ME coupling. Analysis of the spot intensity distribution in the RSM patterns of $(-1\ 1\ 3)$ and $(1\ -1\ 3)$ reflections (Supplementary Figure S2) suggests that the 109° ferroelastic switching (from $r1^+$ to $r2^-/r4^-$ or from $r2^+/r4^+$ to $r3^-/r1^-$) occurs in up to 23% of the entire probed area.

By using this effect, the ferroelectric/ferroelastic domain switching-induced strong ME coupling and non-volatile tuning of magnetism in FeGaB/PZN-PT (001) are demonstrated as shown in Figures 1d–f. We use the shift of the FMR field (H_r) to quantitatively determine the electric field-induced effective magnetic anisotropic field (H_{eff}), where $H_{eff} = |\Delta H_r|$. Details are described in Supplementary Information (Supplementary Figures S5 and S6). As shown in Figure 1d, the

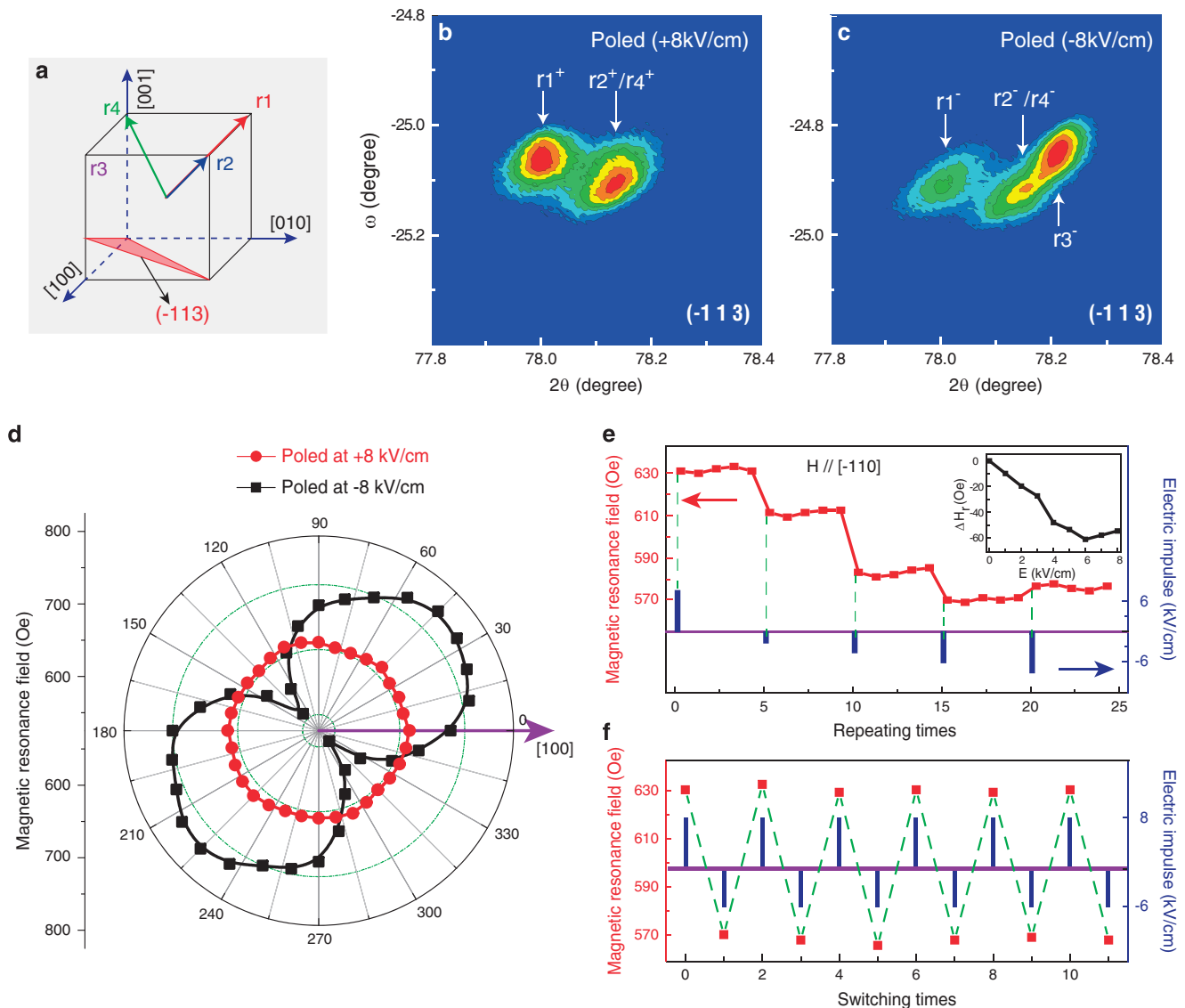


Figure 1 Ferroelectric domain switching and non-volatile tuning of magnetism in FeGaB/PZN-PT(001). (a–c) Schematics of domain structures and reciprocal space maps (RSMs) about the (-113) reflections of the FeGaB/PZN-PT(001) heterostructure under various electric poling states. (d) Angular dependence of ferromagnetic resonance fields under various poling states. A large magnetic anisotropy appears after a negative electric impulse of -8 kV cm^{-1} was applied. (e) Effective magnetic fields along the $[1-10]$ direction as a function of the switching electric impulses, indicating an effective magnetic field tunable range of about 60 Oe. (f) Electric impulse non-volatile switching of effective magnetic anisotropy in FeGaB/PZN-PT (001).

angular dependence of the FMR fields in the FeGaB films deposited on the positively poled (along the $[001]$ direction) PZN-PT (001) substrates exhibits an isotropic nature (red circle). However, as the sample is poled by a negative electric field of -8 kV cm^{-1} , remarkable changes in the FMR field take place and lead to a strong magnetic anisotropy (black curve), indicating an electric impulse-induced magnetic easy axis along the $[110]$ and a hard axis along the $[1-10]$ directions, respectively. This is consistent with the domain structure observation in Figure 1c, where the 109° ferroelastic switching results in a strong lattice strain along the diagonal axes in the (001) plane. We also investigate the effect of a reversed electric impulse on the shift of the resonance fields in the FeGaB/PZN-PT multiferroic heterostructures. As shown in the Figure 1e, various negative switching impulses enable the change in the resonance fields, implying that the magnitude of the electric impulse influences the polarization switching pathways. The robust electrically controlled non-volatile switching of

the resonance field is demonstrated by applying a positive impulse of 8 kV cm^{-1} along the $[001]$ direction and a negative impulse of -6 kV cm^{-1} alternatively (Figure 1f). A stable and repeatable tuning of magnetic resonance field up to $\Delta H_r = 64 \text{ Oe}$ is obtained, indicating that the electric impulse can indeed non-volitely switch the magnetism in FeGaB/PZN-PT(001) via the 109° ferroelectric domain switching. We anticipate such electric tuning of magnetism can still remain robust after thousands of times of 109° ferroelectric domain switching, according to a similar report in the CoFeB/PMN-PT (001) heterostructure.¹⁸

In the (011) -oriented PZN-PT substrates, the polarization switching pathways are quite different from those permitted in the (001) -oriented PZN-PT. As the ferroelastic domains $r1/r2$ and $r3/r4$ possess the different reciprocal lattices along the $[0HH]$ direction, these two domain states can be distinguished by the spot location in the (022) reflection. As the FeGaB/PZN-PT (011) heterostructure is vertically

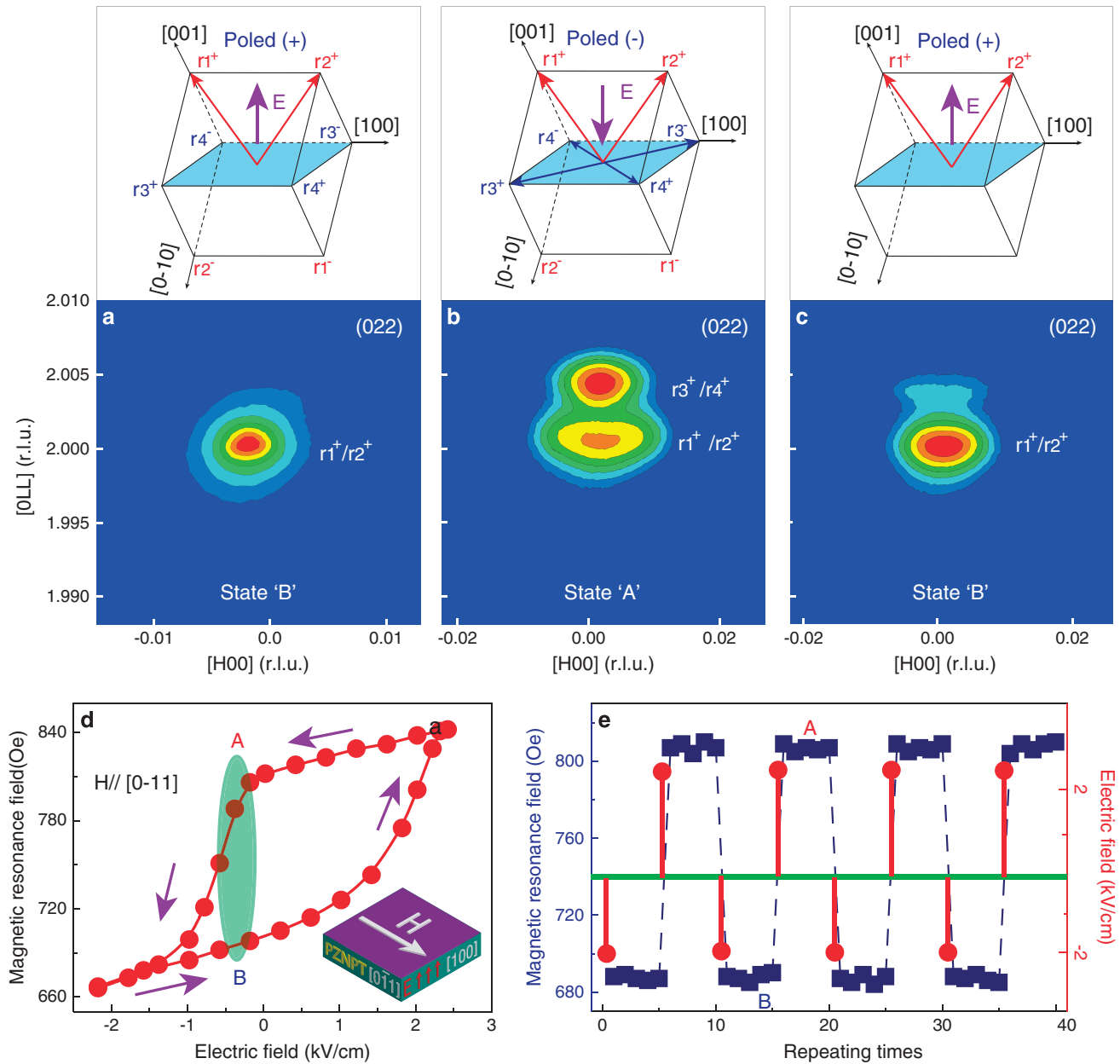


Figure 2 Ferroelectric domain switching and non-volatile tuning of magnetism in FeGaB/PZN-PT (011). (a–c) Schematic domain structures and reciprocal space maps (RSMs) about the (022) reflection of the FeGaB/PZN-PT(001) under various electric poling states. (d) A hysteresis loop of the resonance field as a function of applied electric fields. A and B represent two distinct magnetic remnant states. (e) Electric impulse-induced non-volatile switching of magnetic anisotropy between the distinct states A and B. The magnetic resonance measurement was repeated five times for each applied impulse.

poled with a strong positive electric impulse of 8 kV cm^{-1} , the RSM pattern of the (022) reflection displays a single spot with a lower reciprocal lattice value, corresponding to the $r1/r2$ domain structure (Figure 2a). This suggests a fully out-of-plane polarization (Figure 2a). Upon poling the sample with a small negative field of -2.5 kV cm^{-1} , which is close to the coercive field of the PZN-PT (011) crystal, the polarization is reversed from the out-of-plane direction to the in-plane direction, indicating a 71° ferroelastic domain switching from $r1/r2$ to $r3/r4$ (Figure 2b). In this process, strong lattice strains along the $[011]$ and $[0-11]$ directions are produced, which is confirmed by the distinct spot separation in the (022) reflection, arising from the difference in the d-spacing between the $r1/r2$ and $r3/r4$ domain states. As a positive electric field of 8 kV cm^{-1} is

reapplied, the polarization is switched back to the out-of-plane direction and stays in the $r1/r2$ state (Figure 2c). Therefore, a stable and reversible ferroelectric/ferroelastic domain switching pathway is created and results in a large lattice strain along the $[011]$ and $[0-11]$ directions. Based upon the analysis of the RSM patterns in the vicinity of the (022) and (222) reflections (as shown in Supplementary Figure S3), the 71° ferroelastic switching takes place in up to 80% of the poled area. This switching is much more efficient than that obtained in the (001)-oriented PZN-PT, where only 23% of the entire probed area is involved to contribute a lattice strain.

Figure 2d shows the hysteresis loop of resonance field as a function of electric field measured along the in-plane $[0-11]$ direction. In the beginning, the sample is negatively poled to saturation with the

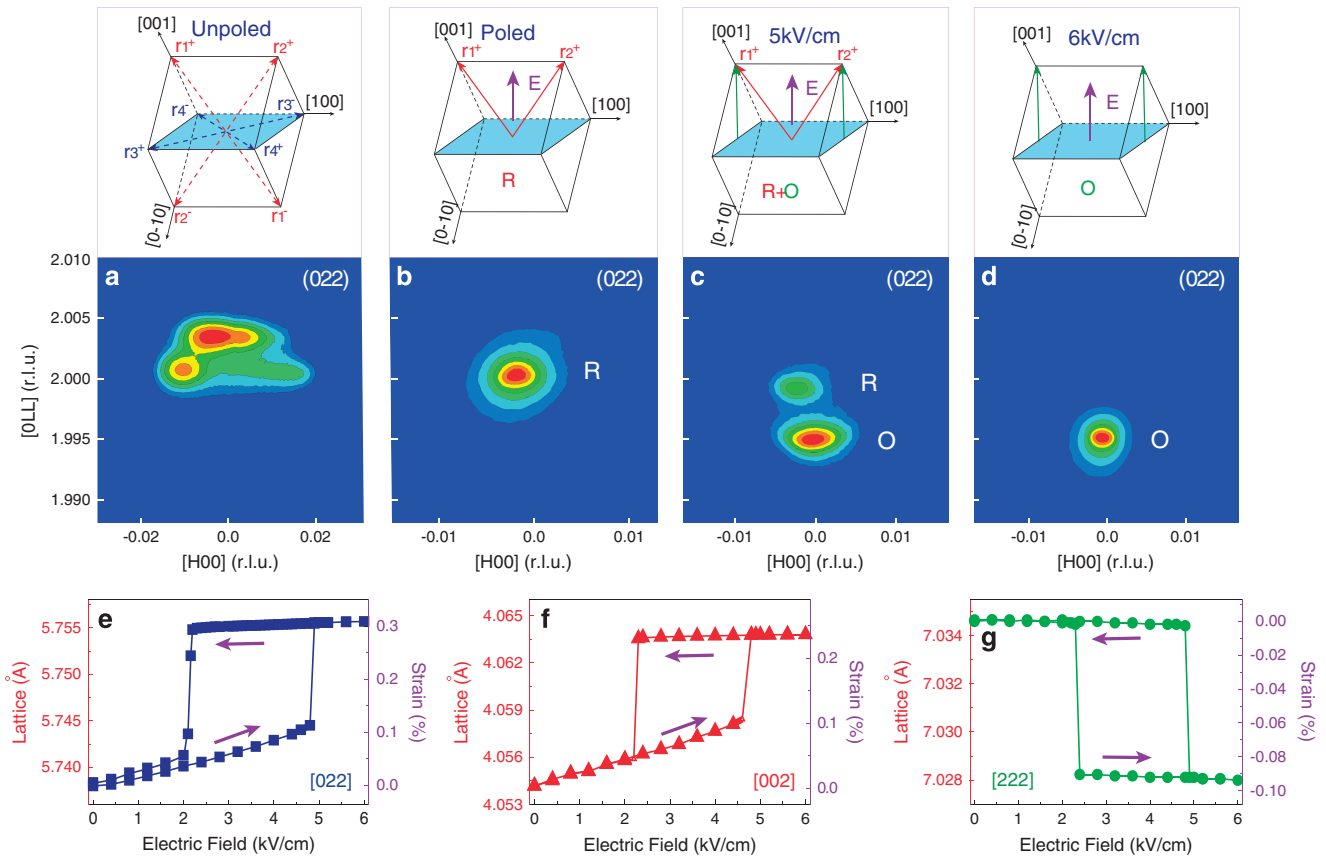


Figure 3 Voltage-induced ferroelectric phase change. (a–d) Schematics of domain structures and reciprocal space maps (RSMs) about the (022) reflections of FeGaB/PZN-PT(011) with the application of various electric impulses. (e–g) Hysteresis loops of the lattice parameters as a function of the electric field along the various directions of [022], [002] and [222], showing large lattice strains of 0.3%, 0.24% and 0.09%, respectively.

polarization pointing downward. Upon applying a positive electric field on the sample, a remarkable resonance field jump takes place at the coercive field of 2.5 kV cm^{-1} . In this process, the polarization switching from the out-of-plane to the in-plane direction enables a strong lattice strain and ME coupling along the in-plane [0-11] direction. As the electric field is ramped to the negative range, a sudden drop of the resonance field takes place. Thus, a complete bipolar electric field cycle leads to a hysteresis loop with two distinct remnant states A and B, which are stable and switchable, reminiscent of magnetic memory. Figure 2e shows the electric impulse non-volatile tuning of the FMR field or magnetic anisotropy in FeGaB/PZN-PT (011) under multiple cycles. As the sample was negatively poled with an electric impulse of -2 kV cm^{-1} , the remnant state A remains and shows a minimum resonance field of 680 Oe. Upon applying a positive electric impulse of 2.5 kV cm^{-1} , the resonance field switches to 810 Oe and remains in state B, with $\Delta H_r = 123 \text{ Oe}$. Therefore, electrically control of non-volatile switching of magnetic anisotropy or resonance field is realized by properly alternating the polarity of the applied electric impulse applied on to FeGaB/PZN-PT(011).

Electric field-induced phase transition is a common phenomenon in single-crystal ferroelectrics. In (011)-oriented PZN-(6–7%)PT slab, a rhombohedral-to-orthorhombic phase transition takes place under a sufficiently high poling field applied along the [011] direction, with the magnitude critical triggering electric field varying slightly with the PbTiO_3 (PT) composition. The crystal would return to the rhombohedral phase if the field was removed. Such electric field-induced phase transition can generate large lattice strain for the switching of

magnetism in multiferroic FeGaB/PZN-PT (011) heterostructures. Figure 3 shows the electric field dependence of the RSM patterns in the vicinity of the (022) reflection and the lattice changes along various crystallographic directions of the PZN-PT(011). Electric field-dependent RSM patterns of the (002) and (222) reflections are shown in Supplementary Figure S4. In the initial state, the RSM patterns suggest a rhombohedral domain structure with the electric polarization pointing to the eight possible body diagonal directions (Figure 3a). After positively poling the sample, the RSM patterns of the (022) reflection exhibit a rhombohedral domain structure with the electric polarization pointing to upward (Figure 3b). Upon increasing the electric field to 5 kV cm^{-1} , an addition spot appears in the RSM patterns, indicating the coexistence of an orthorhombic and the rhombohedral phases (Figure 3c). Because PZN-PT(011) shows a larger c axis in its orthorhombic lattice, the spots with smaller reciprocal lattice parameters represent the orthorhombic phase. Upon increasing the electric field to 6 kV cm^{-1} , the rhombohedral phase disappears, leading to a pure orthorhombic phase as only one spot remains in the (022) reflection (Figure 3d). In this process, the polarization is completely switched from the body diagonal $\langle 111 \rangle$ directions to the plane diagonal $\langle 011 \rangle$ directions. Figures 3d–f) show the hysteresis loops of the lattice parameters as a function of the electric fields along the [100], [011] and [111] directions, respectively. As the electric field exceeds the threshold strength of 5 and 2 kV cm^{-1} , sharp changes in the lattice parameters take place, reaching 0.3%, 0.23% and 0.08% along the [011], [001] and [111] directions, respectively. This suggests that the field-induced phase transition from

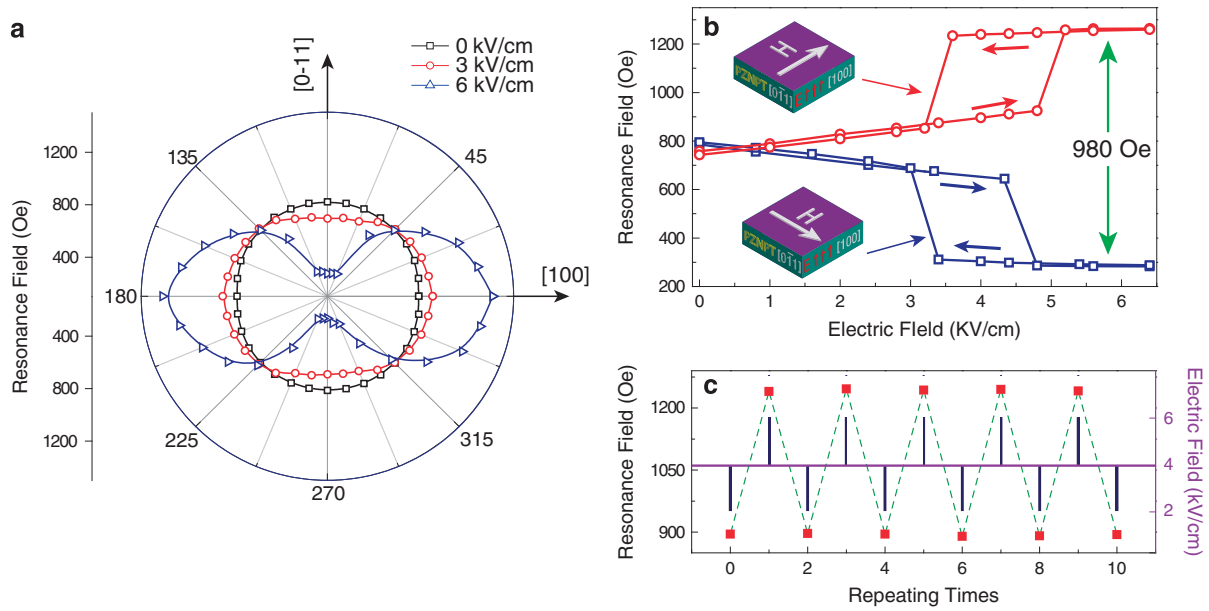


Figure 4 Tuning of magnetism by ferroelectric phase transition in FeGaB/PZN-PT (011). (a) Angular dependence of the ferromagnetic resonance field under various poled states. (b) Hysteresis loops of resonance fields as a function of electric field applied along the [100] (red) and the [0-11] (blue) directions, respectively. (c) Electric impulse switching of magnetism in FeGaB/PZN-PT (011).

the rhombohedral to orthorhombic phase in PZN-PT results in a dramatic elongation in the [011] direction.

Figure 4 shows the structural phase transition-induced switching of magnetization. According to the angular-dependent magnetic resonance field, a uniaxial magnetic easy axis along the [0-11] direction appears when the applied electric field is above the threshold magnitude of phase transition (Figure 4a). Hysteresis loops of the resonance field versus electric field measured along the [100] and [0-11] directions are shown in Figure 4b, exhibiting a large magnetic anisotropy field tunable range of up to 980 Oe. The fields needed to switch between the distinct rhombohedral and orthorhombic phases are determined to be 4.8 kV cm^{-1} (R–O) and 3.5 kV cm^{-1} (O–R). In the presence of a 4-kV cm^{-1} bias electric field, non-volatile switching of magnetization is realized by applying electric impulses of 6 and 2 kV cm^{-1} alternately on the sample of FeGaB/PZN-PT (011) (Figure 4c). The change of resonance magnetic field, $\Delta H_r = 498 \text{ Oe}$, is approximately four times larger than the 123 Oe induced by 71° polarization switching in FeGaB/PZN-PT (011), and approximately eight times larger than the 64 Oe induced by 109° polarization switching in FeGaB/PZN-PT (001). E-field dependence of magnetic hysteresis loops were investigated as shown in Figure S7. Table 1 summarizes the changes of resonance field for these three cases. For the voltage-induced ferroelastic domain switching, the average in-plane strains induced by 71° or 109° switching can be estimated by multiplying the nominal lattice deformation associated with 71° or 109° switching by the percentage of ferroelectric domains that experienced 71° or 109° switching, respectively. Such percentages are extracted from RSM patterns. While in the case of voltage-induced Rhombohedral to Orthorhombic (R–O) phase transition, the average strain is calculated from the experimentally measured lattice deformation (Figures 3e–g). In particular, the change of effective magnetic anisotropy field (ΔH_{eff}) calculated based on these voltage-induced strains agrees fairly well with the experimentally measured ΔH_r (see Table 1).

The voltage-induced average strains in these three cases are further fed into a phase-field model (see Methods section) to computationally

Table 1 Comparison of experimental and simulation results on ferroelectric domain switching and phase transition-induced effective magnetic fields

	FeGaB/PZN-PT (001) (Oe)	FeGaB/PZN-PT (011) domain switching (Oe)	FeGaB/PZN-PT (011) phase transition (Oe)
ΔH_r (experiment)	64	123	498
ΔH_{eff} (simulation)	68.93	120.29	416

visualize the possible changes in magnetic domain structure under zero magnetic field, complementary to the experimentally observed changes of magnetic properties.⁵⁸ Note that the use of average strain as the model input is reasonable only when the average size of one single magnetic domain in the FeGaB film is sufficiently large to cover many of the ferroelectric domains on the PMN-PT surface, otherwise one may use the nominal domain switching-induced lattice deformation as the input. Starting from random magnetization distribution, an almost uniform magnetization distribution is obtained at equilibrium under zero strain, and is further evolved to new equilibrium state upon applying the strain transferred from the PMN-PT substrate. Figure 5 shows the initial magnetization distribution, and the stable magnetization distributions corresponding to different polarization rotation paths or the rhombohedral to orthorhombic (R–O) phase transition. First, the 109° polarization rotation in PZN-PT (001) would induce a non-volatile shear strain (average strain from the entire PZN-PT surface, the same definition is applicable to the strain mentioned below unless otherwise stated) of about -0.04% within the (001) plane, which is equivalent to biaxial normal strains of $\varepsilon_{[110]} \approx -0.04\%$, $\varepsilon_{[1-10]} \approx 0.04\%$ (represented by the dashed arrows in the bottom panel of Figure 5a). Given the positive magnetostriction coefficient of FeGaB, the magnetization would preferably align along the [1-10] axis, consistent with the simulation results (the middle panel of Figure 5a). Second, the 71° polarization rotation path in PZN-PT (011) would induce a non-volatile normal strain of about

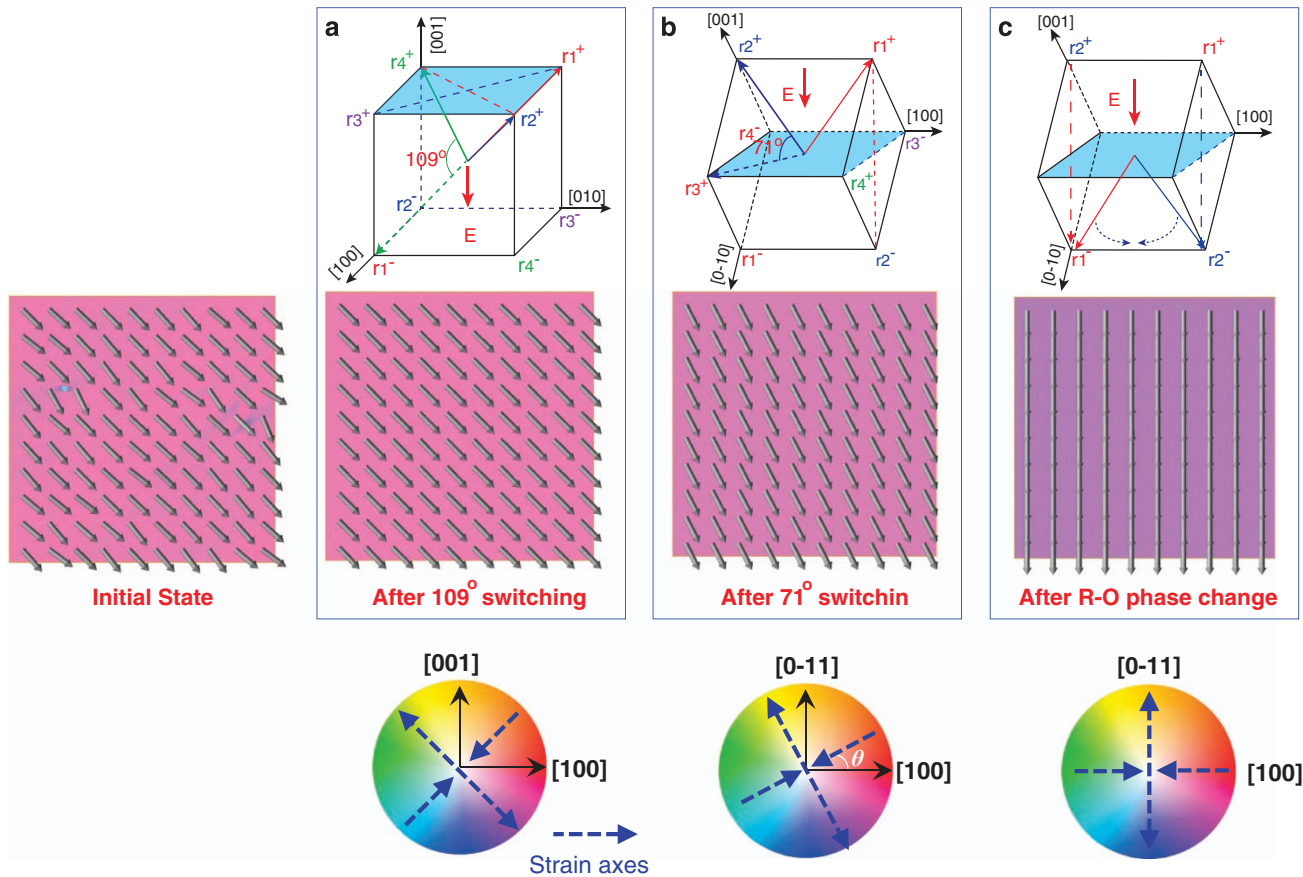


Figure 5 Magnetic domain response to strains induced by ferroelectric domain switching/phase transition. Stable surface local magnetization distributions in the amorphous FeGaB film after applying a downward electric field (E) to reverse the polarization in the (a), (001)-oriented, and (b), (011)-oriented rhombohedral PZN-PT crystals underneath and (c), to induce the rhombohedral to orthogonal (R–O) ferroelectric phase transition in the (011)-oriented PZN-PT. The initial local magnetization distribution ($1 \times 1 \mu\text{m}$) is obtained starting from random magnetization distribution, and is then evolved to a new stable structure upon applying various strains. The dashed arrows in the color wheels indicate the strain axes, where the double-headed (head-to-head) arrows indicate tensile (compressive) strains. We assume the average size of the magnetic domain in such 50-nm-thick FeGaB film is considerably larger than the average size of ferroelectric domain on the PZN-PT surface.

0.14% along the $[0-11]$ axis, along with a non-volatile shear strain of 0.099% (or -0.099%) within the (011) plane. Specifically, if the polarization rotates to r_3 (r_4), the shear strain would be negative (positive). Such tensile normal strain and negative shear strains are equivalent to the biaxial tensile (about 0.19%) and compressive (about -0.05%) strains along the axes shown at the bottom of Figure 5b, where the deviation angle (θ) is about 27.4° . This is consistent with the simulated local magnetization distribution (the middle panel of Figure 5b). Local magnetization distribution after polarization rotation to r_4 would be a mirror-symmetry distribution of the present one with $[0-11]$ being the symmetric axis. Third, the electrically induced R–O phase transition in PZN-PT (011) would induce a large, volatile (bistable under a bias electric field, compare Figures 3e–g) strain in the (011) plane (that is, $\varepsilon_{[0-11]} \approx 0.47\%$ and $\varepsilon_{[100]} \approx -0.48\%$), as shown in the bottom panel of Figure 5c. As a result, the local magnetization vectors would rotate to the $[0-11]$ axis. Note that these simulation results only explore one possibility of the changes of local magnetization distribution, by assuming that the average magnetic domain size is considerably larger than ferroelectric domains and by neglecting the influence of growth-induced strains in such relatively thick (50 nm) and amorphous magnetic film. More accurate predictions can be made with a known magnetic domain structure in the as-grown magnetic film from experimental measurements.

In conclusion, three viable routes have been systematically demonstrated, which allow us to realize electric field-induced non-volatile switching of magnetism in the FeGaB/PZN-PT heterostructures via electrically non-volatile ferroelastic domain switching. Various ferroelastic domain switching pathways have been explored to achieve a strong and homogeneous non-volatile ME coupling. The results show that the 109° ferroelastic/ferroelectric switching in the (001)-oriented FeGaB/PZN-PT (001) only occurs in 23% of the entire probed area, which may cause inhomogeneous in-plane strain with the lack of the switching control due to the competition among the polarization reversals. In contrast, in the FeGaB/PZN-PT (011), the 71° ferroelastic/ferroelectric switching can occupy up to 80% of the entire probed area, leading to a more homogeneous and controllable lattice strain with larger magnitude on average and thereby a strong non-volatile ME coupling effect. In addition, the electric impulse-induced ferroelectric phase transition in the (011)-oriented PZN-PT is also able to switch the distinct magnetic states in the mechanically coupled FeGaB films. In particular, the much stronger non-volatile ME coupling, demonstrated by the much larger changes in both the magnetic resonance field and magnetic domain structure, is due to the large lattice deformation arising from the phase transition. This work provides a platform for exploring the electrically controlled non-volatile tuning of order parameters that are coupled to the lattice strain in thin-film heterostructures.

CONFLICT OF INTEREST

The authors declare no conflict of interest.

ACKNOWLEDGEMENTS

The work was supported by the Natural Science Foundation of China (Grant No. 51472199, 11534015), Natural Science Foundation of Shaanxi Province (Grant No. 2015JM5196), the National 111 Project of China (B14040), the 973 program (Grant No. 2015CB057402) and the Fundamental Research Funds for the Central Universities. Ming Liu was supported by the China Recruitment Program of Global Youth Experts. The work at Penn State is supported by the National Science Foundation under Grant No. DMR-1410714.

Author contributions: ML, TN and J-MH equally contributed to this work. ML initialized the idea and planned the experiments. ML, TN made the samples and performed all measurements. J-MH did the simulation. All authors discussed the results and commented on the manuscript.

- Eerenstein, W., Mathur, N. D. & Scott, J. F. Multiferroic and magnetoelectric materials. *Nature* **442**, 759–765 (2006).
- Ohno, H. A window on the future of spintronics. *Nat. Mater.* **9**, 952–954 (2010).
- Wu, S. M., Cybart, S. A., Yu, P., Rossell, M. D., Zhang, J. X., Ramesh, R. & Dynes, R. C. Reversible electric control of exchange bias in a multiferroic field-effect device. *Nat. Mater.* **9**, 756–761 (2010).
- Kleemann, W. Switching magnetism with electric fields. *Physics* **2**, 105 (2009).
- Spaldin, N. A., Cheong, S. W. & Ramesh, R. Multiferroics: past, present, and future. *Phys. Today* **63**, 38–43 (2010).
- Baek, S. H., Jang, H. W., Folkman, C. M., Li, Y. L., Winchester, B., Zhang, J. X., He, Q., Chu, Y. H., Nelson, C. T., Rzechowski, M. S., Pan, X. Q., Ramesh, R., Chen, L. Q. & Eom, C. B. Ferroelastic switching for nanoscale non-volatile magnetoelectric devices. *Nat. Mater.* **9**, 309–314 (2010).
- Scott, J. F. Data storage. Multiferroic memories. *Nat. Mater.* **6**, 256–257 (2007).
- Ahn, C. H., Triscone, J. M. & Mannhart, J. Electric field effect in correlated oxide systems. *Nature* **424**, 1015–1018 (2003).
- Cao, J., Ertekin, E., Srinivasan, V., Fan, W., Huang, S., Zheng, H., Yim, J. W., Khanal, D. R., Ogletree, D. F., Grossman, J. C. & Wu, J. Strain engineering and one-dimensional organization of metal-insulator domains in single-crystal vanadium dioxide beams. *Nat. Nano.* **4**, 732–737 (2009).
- Infante, I. C., Lisenkov, S., Dupé, B., Bibes, M., Fusil, S., Jacquet, E., Geneste, G., Petit, S., Courtial, A., Juraszek, J., Bellaiche, L., Barthélémy, A. & Dkhil, B. Bridging multiferroic phase transitions by epitaxial strain in BiFeO₃. *Phys. Rev. Lett.* **105**, 057601 (2010).
- Vaz, C. A. F., Hoffman, J., Anh, C. H. & Ramesh, R. Magnetoelectric coupling effects in multiferroic complex oxide composite structures. *Adv. Mater.* **22**, 2900–2918 (2010).
- Dong, S. X., Zhai, J. Y., Li, J. F. & Viehland, D. Small dc magnetic field response of magnetoelectric laminate composites. *Appl. Phys. Lett.* **88**, 082907 (2006).
- Nan, C. W., Bichurin, M. I., Dong, S. X., Viehland, D. & Srinivasan, G. Multiferroic magnetoelectric composites: historical perspective, status, and future directions. *J. Appl. Phys.* **103**, 031101 (2008).
- Liu, M., Obi, O., Lou, J., Chen, Y. J., Cai, Z. H., Stoute, S., Espanol, M., Lew, M., Situ, X., Ziemer, K. S., Harris, V. G. & Sun, N. X. Giant electric field tuning of magnetic properties in multiferroic ferrite/ferroelectric heterostructures. *Adv. Funct. Mater.* **19**, 1826–1831 (2009).
- Das, J., Song, Y. Y., Mo, N., Krivosik, P. & Patton, C. E. Electric-field-tunable low loss multiferroic ferrimagnetic-ferroelectric heterostructures. *Adv. Mater.* **21**, 2045–2049 (2009).
- Ramesh, R. & Spaldin, N. A. Multiferroics: progress and prospects in thin films. *Nat. Mater.* **6**, 21–29 (2007).
- Zheng, R., Jiang, Y., Wang, Y., Chan, H., Choy, C. & Luo, H. Ferroelectric poling and converse-piezoelectric-effect-induced strain effects in La_{0.7}Ba_{0.3}MnO₃ thin films grown on ferroelectric single-crystal substrates. *Phys. Rev. B* **79**, 1–7 (2009).
- Zhang, S., Zhao, Y. G., Li, P. S., Yang, J. J., Rizwan, S., Zhang, J. X., Seidel, J., Qu, T. L., Yang, Y. J., Luo, Z. L., He, Q., Zou, T., Chen, Q. P., Wang, J. W., Yang, L. F., Sun, Y., Wu, Y. Z., Xiao, X., Jin, X. F., Huang, J., Gao, C., Han, X. F. & Ramesh, R. Electric-field control of nonvolatile magnetization in structure at room temperature. *Phys. Rev. Lett.* **108**, 137203 (2012).
- Liu, M., Hoffman, J., Wang, J., Zhang, J., Nelson-Cheeseman, B. & Bhattacharya, A. Non-volatile ferroelastic switching of the Verwey transition and resistivity of epitaxial Fe₃O₄/PMN-PT (011). *Sci. Rep.* **3**, 1876 (2013).
- Liu, M., Howe, B. M., Grazulis, L., Mahalingam, K., Nan, T., Sun, N. X. & Brown, G. J. Voltage-impulse-induced non-volatile ferroelastic switching of ferromagnetic resonance for reconfigurable magnetoelectric microwave devices. *Adv. Mater.* **25**, 4886–4892 (2013).
- Liu, M., Zhou, Z., Nan, T., Howe, B. M., Brown, G. J. & Sun, N. X. Voltage tuning of ferromagnetic resonance with bistable magnetization switching in energy-efficient magnetoelectric composites. *Adv. Mater.* **25**, 1435–1439 (2013).
- Schlom, D. G., Chen, L. Q., Eom, C. B., Rabe, K. M., Streiffer, S. K. & Triscone, J. M. Strain tuning of ferroelectric thin films. *Ann. Rev. Mater. Res.* **37**, 589–626 (2007).
- Tsymbal, E. Y. & Kohlstedt, H. Applied physics - tunneling across a ferroelectric. *Science* **313**, 181–183 (2006).
- Liu, M. & Sun, N. X. Voltage control of magnetism in multiferroic heterostructures. *Philos. Trans. R. Soc. A Math. Phys. Eng. Sci.* **372**, 20120439 (2014).
- Srinivasan, G. & Fetisov, Y. K. Ferrite-piezoelectric layered structures: microwave magnetoelectric effects and electric field tunable devices. *Ferroelectrics* **342**, 65–71 (2006).
- Dho, J. H., Qi, X. D., Kim, H., MacManus-Driscoll, J. L. & Blamire, M. G. Large electric polarization and exchange bias in multiferroic BiFeO₃. *Adv. Mater.* **18**, 1445 (2006).
- Ma, J., Hu, J. M., Li, Z. & Nan, C. W. Recent progress in multiferroic magnetoelectric composites: from bulk to thin films. *Adv. Mater.* **23**, 1062–1087 (2011).
- Hu, J. M., Chen, L. Q. & Nan, C. W. Multiferroic heterostructures integrating ferroelectric and magnetic materials. *Adv. Mater.* **28**, 15–39 (2016).
- Yang, X., Zhou, Z., Nan, T., Gao, Y., Yang, G. M., Liu, M. & Sun, N. X. Recent advances in multiferroic oxide heterostructures and devices. *J. Mater. Chem. C* **4**, 234–243 (2016).
- Liu, M., Obi, O., Cai, Z. H., Lou, J., Yang, G. M., Ziemer, K. S. & Sun, N. X. Electrical tuning of magnetism in Fe₃O₄/PZN-PT multiferroic heterostructures derived by reactive magnetron sputtering. *J. Appl. Phys.* **107**, 073916 (2010).
- Hu, J.-M. & Nan, C. W. Electric-field-induced magnetic easy-axis reorientation in ferromagnetic/ferroelectric layered heterostructures. *Phys. Rev. B* **80**, 224416 (2009).
- Fetisov, Y. K. & Srinivasan, G. Electric field tuning characteristics of a ferrite-piezoelectric microwave resonator. *Appl. Phys. Lett.* **88**, 142503–143503-3 (2006).
- Zhao, P., Zhao, Z. L., Hunter, D., Suchoski, R., Gao, C., Mathews, S., Wuttig, M. & Takeuchi, I. Fabrication and characterization of all-thin-film magnetoelectric sensors. *Appl. Phys. Lett.* **94**, 243507 (2009).
- Thiele, C., Dörr, K., Bilani, O., Rödel, J. & Schultz, L. Influence of strain on the magnetization and magnetoelectric effect in La_{0.7}A_{0.3}MnO₃/PMN-PT(001) (A=Sr,Ca). *Phys. Rev. B* **75**, 054408 (2007).
- Sahoo, S., Polisetty, S., Duan, C. G., Jaswal, S. S., Tsymbal, E. Y. & Binek, C. Ferroelectric control of magnetism in BaTiO₃/Fe heterostructures via interface strain coupling. *Phys. Rev. B* **76**, 092108 (2007).
- Liu, M. Novel Laminated multiferroic heterostructures for reconfigurable microwave devices. *Chin Sci Bull.* **59**, 5180–5190 (2014).
- Venkataiah, G., Wada, E., Taniguchi, H., Itoh, M. & Taniyama, T. Electric-voltage control of magnetism in Fe/BaTiO₃ heterostructured multiferroics. *J. Appl. Phys.* **113**, 17C701 (2013).
- Wu, T., Zhao, P., Bao, M., Bur, A., Hockel, J. L., Wong, K., Mohanchandra, K. P., Lynch, C. S. & Carman, G. P. Domain engineered switchable strain states in ferroelectric (011) [Pb(Mg_{1/3}Nb_{2/3})O₃]_(1-x)[PbTiO₃]_x (PMN-PT, x≈0.32) single crystals. *J. Appl. Phys.* **109**, 124101 (2011).
- Bennett, S. P., Wong, A. T., Glavic, A., Herklotz, A., Urban, C., Valmianski, I., Biegalski, M. D., Christen, H. M., Ward, T. Z. & Lauter, V. Giant controllable magnetization changes induced by structural phase transitions in a metamagnetic artificial multiferroic. *Sci. Rep.* **6**, 22708 (2016).
- Buzzi, M., Chopdekar, R. V., Hockel, J. L., Bur, A., Wu, T., Pilet, N., Warnicke, P., Carman, G. P., Heyderman, L. J. & Nolting, F. Single domain spin manipulation by electric fields in strain coupled artificial multiferroic nanostructures. *Phys. Rev. Lett.* **111**, 027204 (2013).
- Shirahata, Y., Nozaki, T., Venkataiah, G., Taniguchi, H., Itoh, M. & Taniyama, T. Switching of the symmetry of magnetic anisotropy in Fe/BaTiO₃ heterostructures. *Appl. Phys. Lett.* **99**, 022501 (2011).
- Lou, J., Liu, M., Reed, D., Ren, Y. H. & Sun, N. X. Giant electric field tuning of magnetism in novel multiferroic fegab/lead zinc niobate-lead titanate (pzn-pt) heterostructures. *Adv. Mater.* **21**, 4711 (2009).
- Liu, M., Obi, O., Lou, J., Stoute, S., Huang, J. Y., Cai, Z. H., Ziemer, K. S. & Sun, N. X. Spin-spray deposited multiferroic composite Ni(0.23)Fe(2.77)O(4)/Pb(Zr,Ti)O(3) with strong interface adhesion. *Appl. Phys. Lett.* **92**, 152504 (2008).
- Martin, L. W., Chu, Y. H., Holcomb, M. B., Huijben, M., Yu, P., Han, S. J., Lee, D., Wang, S. X. & Ramesh, R. Nanoscale control of exchange bias with BiFeO₃ thin films. *Nano. Lett.* **8**, 2050–2055 (2008).
- Hu, J.-M., Li, Z., Chen, L.-Q. & Nan, C.-W. High-density magnetoresistive random access memory operating at ultralow voltage at room temperature. *Nat. Commun.* **2**, 553 (2011).
- Liu, M., Li, S., Zhou, Z., Beguhn, S., Lou, J., Xu, F., Jian, Lu, T. & Sun, N. X. Electrically induced enormous magnetic anisotropy in Terfenol-D/lead zinc niobate-lead titanate multiferroic heterostructures. *J. Appl. Phys.* **112**, 063917 (2012).
- Wu, T., Bur, A., Zhao, P., Mohanchandra, K. P., Wong, K., Wang, K. L., Lynch, C. S. & Carman, G. P. Giant electric-field-induced reversible and permanent magnetization reorientation on magnetoelastic Ni(011) [Pb(Mg_{1/3}Nb_{2/3})O₃]_[sub 3] [sub (1-x)]-[PbTiO₃]_[sub 3] heterostructure. *Appl. Phys. Lett.* **98**, 012504–012503 (2011).
- Rata, A. D., Herklotz, A., Nenkov, K., Schultz, L. & Dörr, K. Strain-induced insulator state and giant gauge factor of La_{0.7}Sr_{0.3}CoO₃ films. *Phys. Rev. Lett.* **100**, 076401 (2008).
- Zheng, R. K., Jiang, Y., Wang, Y., Chan, H. L. W., Choy, C. L. & Luo, H. S. Investigation of substrate-induced strain effects in La_{0.7}Ca_{0.15}Sr_{0.15}MnO₃ thin films using ferroelectric polarization and the converse piezoelectric effect. *Appl. Phys. Lett.* **93**, 102904 (2008).
- Wu, T., Bur, A., Wong, K., Zhao, P., Lynch, C. S., Amiri, P. K., Wang, K. L. & Carman, G. P. Electrical control of reversible and permanent magnetization

- reorientation for magnetoelectric memory devices. *Appl. Phys. Lett.* **98**, 262504 (2011).
- 51 Hu, J. M., Li, Z., Wang, J. & Nan, C. W. Electric-field control of strain-mediated magnetoelectric random access memory. *J. Appl. Phys.* **107**, 093912 (2010).
- 52 Parkes, D. E., Cavill, S. A., Hindmarch, A. T., Wadley, P., Mcgee, F., Staddon, C. R., Edmonds, K. W., Campion, R. P., Gallagher, B. L. & Rushforth, A. W. Non-volatile voltage control of magnetization and magnetic domain walls in magnetostrictive epitaxial thin films. *Appl. Phys. Lett.* **101**, 072402 (2012).
- 53 Aizu, K. Possible species of ferromagnetic, ferroelectric, and ferroelastic crystals. *Phys. Rev. B* **2**, 754–772 (1970).
- 54 Abo, G. S., Hong, Y. K., Park, J., Lee, J., Lee, W. & Choi, B. C. Definition of magnetic exchange length. *IEEE Trans. Magn.* **49**, 4937–4939 (2013).
- 55 Hu, J. M., Yang, T. N., Chen, L. Q. & Nan, C. W. Engineering domain structures in nanoscale magnetic thin films via strain. *J. Appl. Phys.* **114**, 164303 (2013).
- 56 Lou, J., Insignares, R. E., Cai, Z., Ziemer, K. S., Liu, M. & Sun, N. X. Soft magnetism, magnetostriction, and microwave properties of FeGaB thin films. *J. Appl. Phys.* **91**, 182504 (2007).
- 57 Morley, N. A., Javed, A. & Gibbs, M. R. J. Effect of a forming field on the magnetic and structural properties of thin Fe–Ga films. *J. Appl. Phys.* **105**, 07A912 (2009).
- 58 Hu, J. M., Sheng, G., Zhang, J. X., Nan, C. W. & Chen, L. Q. Phase-field simulation of strain-induced domain switching in magnetic thin films. *Appl. Phys. Lett.* **98**, 112505 (2011).



This work is licensed under a Creative Commons Attribution 4.0 International License. The images or other third party material in this article are included in the article's Creative Commons license, unless indicated otherwise in the credit line; if the material is not included under the Creative Commons license, users will need to obtain permission from the license holder to reproduce the material. To view a copy of this license, visit <http://creativecommons.org/licenses/by/4.0/>

© The Author(s) 2016

Supplementary Information accompanies the paper on the NPG Asia Materials website (<http://www.nature.com/am>)